# SIMULATION AND FABRICATION OF Ge ISLANDS ON Si METAL-SEMICONDUCTOR-METAL PHOTODETECTORS

**HADI MAHMODI SHEIKH SARMAST**

**UNIVERSITI SAINS MALAYSIA**

**2010**

# SIMULATION AND FABRICATION OF Ge ISLANDS ON Si METAL-SEMICONDUCTOR-METAL PHOTODETECTORS

**by**

**HADI MAHMODI SHEIKH SARMAST**

**Thesis submitted in fulfilment of the requirements**

**for the degree of**

**Master of Science**

**UNIVERSITI SAINS MALAYSIA**

**November 2010**

## ACKNOWLEDGEMENT

I want to thank God who gave me the hope, faith and love to breathe every day. This dissertation summarized the research work I have accomplished during my master study in Universiti Sains Malaysia. Over these years, I obtained tremendous help from all the people around and I cannot leave the dissertation without expressing my gratitude to them.

First of all and foremost, I would like to thank my supervisor, Assoc. Prof. Md Roslan Hashim, for his all the time support and guidance. I benefited a lot from his valuable guidance, not only in the direction of research, but also in my method of research, which for me was often of greater importance.

I take this unique opportunity to thank school of physics, for providing me the necessary facilities, an excellent academic environment for a successful completion of my work and also Research Grant for supporting this work.

I would also like to express my appreciation to the laboratory assistants in the Nano- Optoelectronics Research Laboratory (NORLAB) for their co-operation, technical assistance, and valuable contribution to my work. The assistance from the staff of the Solid State Physics Laboratory is also acknowledged.

Ultimately, it is the encouragement, understanding, and support of my family, which provided me the courage to embark in this venture.

Lastly, I offer my regards and blessings to all of those who supported me in any respect during the completion of the project.

**TABLE OF CONTENTS** **Page**


| | |
|---|---|
| **ACKNOWLEDGEMENTS** | **ii** |
| **TABLE OF CONTENTS** | **iii** |
| **LIST OF TABLES** | **vii** |
| **LIST OF FIGURES** | **viii** |
| **LIST OF SYMBOLS** | **xiii** |
| **LIST OF ABBREVIATIONS** | **xiv** |
| **ABSTRAK** | **xvi** |
| **ABSTRACT** | **xvii** |

**CHAPTER 1: INTRODUCTION**

| | | |
|---|---|---|
| 1.1 | Overview | 1 |
| 1.2 | Literature Review | 3 |
| | 1.2.1 Ge islands | 3 |
| | 1.2.2 Ge wetting layer | 9 |
| | 1.2.3 Photodetectors | 11 |
| 1.3 | Research Objectives | 15 |
| 1.4 | Organization of Thesis | 15 |

**CHAPTER 2: THEORY**

| | | |
|---|---|---|
| 2.1 | Introduction | 17 |
| 2.2 | Electrical and Optical Properties of Ge | 17 |
| 2.3 | Growth Modes | 23 |
| | 2.3.1 Film growth modes | 23 |
| | 2.3.2 Ge islands growth | 26 |
| | 2.3.3 Ge islands growth from annealed layer | 28 |
| 2.4 | Photodetectors | 29 |
| | 2.4.1 Semiconductor photodetectors | 30 |
| | 2.4.2 Schottky Contact | 33 |
| | 2.4.2(a) Current transport | 35 |

2.4.3 Metal-semiconductor-metal (MSM) photodetector 38
2.5 Summary 41

**CHAPTER 3: EXPERIMENTAL PROCEDURE**

3.1 Introduction 42
3.2 Film Deposition Methods 42
3.2.1 Physical Deposition Methods 43
3.2.1(a) Thermal evaporator 44
3.2.2(b) Sputtering 46
3.3 Instrument 49
3.3.1 Rapid thermal annealing 49
3.4 Fabrication Process 51
3.4.1 Preparation of substrates 51
3.4.2 Deposition of Ge thin films 52
3.4.3 Annealing 52
3.4.4 Characterizations of Ge islands 55
3.4.5 MSM photodetectors fabrication 55
3.5 Simulation 57
3.5.1 ATLAS approach in designing devices 58
3.5.1(a) Physical models of ATLAS-Silvaco 62
3.5.2 Numerical solution procedures in ATLAS 64
3.5.3 Obtaining solution 66
3.6 Summary 66

**CHAPTER 4: THE STUDY OF Ge ISLANDS ON Si MSM PD PERFORMANCE**

4.1 Introduction 67
4.2 Thickness of Deposited Ge Layer 67
4.3 Surface Morphology of Ge Layer by SEM 68
4.4 Energy Dispersive X-ray Spectroscopy (EDX) of Ge Layer 71
4.5 MSM Photodetectors Characteristics 73
4.5.1 Pre-etched MSM photodetector 73
4.5.2 Post-etched MSM photodetector 79

4.6 Summary 83

**CHAPTER 5: SIMULATION OF THE ROLE OF Ge WETTING LAYER IN Si MSM PHOTODETECTOR**

5.1 Introduction 84
5.2 Study of Electron-Hole Current 84
5.3 Study of Carrier Current Density 86
5.4 Study of Carrier Concentration 89
5.5 Study of Current Flow Contour 92
5.6 Study of Electric Field 97
5.7 Study of Transient Responses 98
5.8 Study of Spectral Response 103
5.9 Summary 104

**CHAPTER 6: SIMULATION OF Ge ISLANDS MSM PHOTODETECTOR USING QUANTUM MODEL**

6.1 Introduction 105
6.2 Simulation of Ge Islands MSM PD without Wetting Layer by Quantum Model 105
6.3 Summary 110

**CHAPTER 7: CONCLUSIONS AND RECOMMENDATIONS FOR FUTURE WORK**

7.1 Conclusions 111
7.2 Recommendations for Future Work 114

**REFERENCES** 115

**APPENDICES**

Appendix A SILVACO-ATLAS Code 123

Appendix B The Matlab Code for Calculating Full-Width at Half-Maximum (FWHM) 127

**LIST OF PUBLICATION AND CONFERENCES** 128

## LIST OF TABLES


| | | Page |
|---|---|---|
| Table 2.1 | Band structure parameters for the indirect gap element Germanium. $E_g^{ind}$ is indirect band gap; $E_g^{dir}$ direct band gap at the Γ ; [Streetman *et al.,* 2006]. | 19 |
| Table 2.2 | Phonon energies for germanium at the L point where q $=\frac{\pi}{a}$ (1,1,1), a being the unit cell size. | 23 |
| Table 3.1 | Carrier Generation-Recombination models used in simulation. | 65 |
| Table 3.2 | The electron and hole lifetime values for Ge and Si. | 66 |
| Table 5.1 | Rising time (Tr), falling time (Tf) and FWHM of pre-, post-etched and Si MSM PDs. | 101 |
| Table 6.1 | The electron concentration at the Ge islands/Si substrate. | 111 |

## LIST OF FIGURES


| | | Page |
|---|---|---|
| Figure 2.1 | Crystalline structure of Ge showing the tetrahedral arrangement of the bonds. | 18 |
| Figure 2.2 | Absorption coefficients of Si and Ge [Pavesi *et al.,* 2006]. | 20 |
| Figure 2.3 | Interband transitions in solids: (a) direct band gap, (b) indirect band gap. The vertical arrow represents the photon absorption process, while the wiggly arrow in part (b) represents the absorption or emission of a phonon. | 21 |
| Figure 2.4 | Band structure of Germanium (Energy vs. wave vector) [Fox, 2001]. | 22 |
| Figure 2.5 | Experimental data for the absorption coefficient of germanium at room temperature [Fox, 2001]. | 23 |
| Figure 2.6 | Growth modes of homo-epitaxy: (a) step-propagation, (b) 2d-islands growth, and (c) multi layer growth [Waster, 2005]. | 24 |
| Figure 2.7 | Growth modes of hetero-epitaxy: (a) Frank-van der Merwe (FM) (b) Vollmer-Weber (VM) (c) Stranski-Krastanov (SK) [Waster, 2005]. | 25 |
| Figure 2.8 | Energy band diagram of a metal semiconductor contact [Sze, 2002]. | 35 |
| Figure 2.9 | Basic transport processes over a Schottky-barrier [Sze, 2002]. | 37 |
| Figure 2.10 | Structure of MSM photodetector with interdigitated contacts. | 41 |
| Figure 3.1 | Typical temperature profile in rapid-thermal annealing: solid curve: 1000 ˚C, 10 s anneal; dashed curve: 1100 ˚C spike anneal (zero-time anneal) [Franssila, 2004]. | 52 |
| Figure 3.2 | Typical cross-sectional SEM image showing the typical initial Ge layer on Si. | 54 |
| Figure 3.3 | Temperature profile in rapid-thermal annealing: 30, 45, | 56 |

and 60 s anneals.

| | | |
|---|---|---|
| Figure 3.4 | Fabrication flow of Ge islands and wetting layer Si MSM photodetector. | 58 |
| Figure 3.5 | Schematic diagram of the metal (Ni) pattern used for the evaporation of the MSM structure on top of our Ge/Si stacks. | 59 |
| Figure 3.6 | ATLAS Command Groups with the Primary Statements in each Group. | 61 |
| Figure 3.7 | Mesh assignment for MSM design. | 62 |
| Figure 3.8 | Schematic diagram of the MSM devices simulated in Silvaco (a) pre- etched and (b) post-etched device. | 63 |
| Figure 3.9 | Schematic diagram of the typical pre-etched MSM devices designed in ATLAS. | 64 |
| Figure 4.1 | Cross-sectional SEM image showing the initial (i.e. the as-grown) Ge layer on Si(100). | 69 |
| Figure 4.2 | SEM images of Ge thin film, after RTA at 900 ˚C for 45 s. | 71 |
| Figure 4.3 | EDX spectra of Ge thin film grown on Si, after RTA at 900 ˚C for 45 s. | 74 |
| Figure 4.4 | (a) I-V characteristics of the pre-etched MSM PD for small and large Ge islands and (b) shows the ratio of photocurrent to dark current (current gain). | 76 |
| Figure 4.5 | Schematic of simulated pre-etched MSM photodetector. | 77 |
| Figure 4.6 | Simulated (a) I–V characteristics for Si, Ge small islands and Ge large islands for pre-etched device and (b) shows the ratio of photocurrent to dark current (current gain). | 78 |
| Figure 4.7 | Schematic top view of (a) Ge small islands and (b) large islands showing in metal contact. | 79 |
| Figure 4.8 | Comparison of valence band energy between pre-etched and Si MSM PDs (at 0.5 V bias). | 80 |

| | | |
|---|---|---|
| Figure 4.9 | (a) I-V characteristics of the post-etched MSM PD for small and large Ge islands and (b) shows the ratio of photocurrent to dark current (current gain). | 82 |
| Figure 4.10 | Schematic diagram of the post-etched MSM device. | 84 |
| Figure 4.11 | Simulated (a) I–V characteristics of the MSM photodiode for Si, Ge small islands and Ge large islands for post-etched device and (b) ratio of photocurrent to dark current for post-etched device. | 84 |
| Figure 5.1 | Simulated electron and hole current in pre-etched MSM photodetector. | 87 |
| Figure 5.2 | Simulated electron and hole current in post-etched MSM photodetector. | 87 |
| Figure 5.3 | Simulated electron and hole current density for pre-etched MSM PD under anode (V=0.5 V) through the centre of the islands. | 89 |
| Figure 5.4 | Schematic cross-section of pre-etched MSM PD showing the cut-line. | 89 |
| Figure 5.5 | Simulated electron and hole current density along the Ge wetting layer length from under the anode to under the cathode in pre-etched MSM PD. | 90 |
| Figure 5.6 | Simulated electron and hole current density for post-etched MSM PD under anode (V=0.5 v). | 91 |
| Figure 5.7 | Schematic cross-section of post-etched MSM PD showing the cut-line. | 91 |
| Figure 5.8 | Simulated variation of carrier concentration for pre-etched MSM PD under anode (at 0.5 V bias). | 92 |
| Figure 5.9 | Simulated variation of carrier concentration for post-etched MSM device ( at 0.5V bias). | 93 |
| Figure 5.10 | The part of post-etched MSM PD showing the cut-line through Ge wetting layer beneath the contact. | 93 |
| Figure 5.11 | Simulated carrier concentration for post-etched MSM PD along the Ge wetting layer length under anode (at 0.5 V bias). | 94 |

| | | |
|---|---|---|
| Figure 5.12 | Two-dimensional plot of the current flow in the pre-etched MSM device (at 0.5 V bias). | 95 |
| Figure 5.13 | Simulation of current flow line as function of length in the pre-etched MSM PD ( at 0.5 V bias). | 95 |
| Figure 5.14 | Two-dimensional plot of the simulated current flow in the post-etched MSM PD (at 0.5 V bias). | 96 |
| Figure 5.15 | Simulation of current flow as a function of length in the post-etched MSM PD ( at 0.5 V bias). | 97 |
| Figure 5.16 | Two-dimensional plot of the simulated current flow in the Si MSM PD (at 0.5V bias). | 98 |
| Figure 5.17 | Simulation of current flow as a function of length in the Si MSM PD (at 0.5 V bias). | 98 |
| Figure 5.18 | Simulated electric field profile along the device thickness for pre-etched device at 0.5 V bias. | 99 |
| Figure 5.19 | Simulated electric field profile along the device thickness for post-etched MSM PD at 0.5 V bias. | 100 |
| Figure 5.20 | A nanosecond square-pulse signal applied to the MSM photodetectors to get transient responses. | 101 |
| Figure 5.21 | Simulated transient photocurrent for pre-etched MSM photodetector, showing the 1.17 ns-FWHM. | 102 |
| Figure 5.22 | Simulated transient photocurrent for post-etched MSM photodetector, showing the 1.02 ns-FWHM. | 103 |
| Figure 5.23 | Simulated transient photocurrent for Si MSM photodetector, showing the 1.91 ns-FWHM. | 104 |
| Figure 5.24 | Variation of simulated photocurrent spectra with wavelength for pre-etched, post-etched and Si MSM PDs. | 105 |
| Figure 6.3 | Simulated I-V characteristics of Ge islands Si MSM PD using semi-classical (no quantum effects) and Poisson-Schrodinger (with quantum effects) equations. The size | 110 |

of Ge islands is 20nm width and 10nm height.

Figure 6.4 Simulated electron concentration across nano Ge island calculated with and without quantum confinement model. 111

Figure 6.5 Simulated band gap of Ge and Si substrate. Note that the bandgap of Ge nano island has increased by about 97meV from its bulk value. 112

Figure 6.6 Simulated I-V characteristics for Ge island MSM PD with different sizes calculated using quantum confinement model. Ge islands size are 20nm and 200nm for small and large size respectively. Results from Si MSM are included for comparison. 113

## LIST OF SYMBOLS

| | |
|---|---|
| $E_g$ | Band gap |
| K | Wave vector |
| α | Absorption coefficient |
| $\tau_{n0}$ | Electron lifetime |
| $\tau_{p0}$ | Hole lifetime |
| $T_r$ | Rising time |
| $T_f$ | Falling time |

## LIST OF ABBREVIATIONS

| | |
|---|---|
| S-K | Stranski-Krastanov |
| MBE | Molecular Beam Epitaxy |
| UHV-CVD | Ultra-High Vacuum Chemical Vapor Deposition |
| LPCVD | Low-Pressure Chemical Vapor Deposition |
| MSM | Metal-Semiconductor-Metal |
| PDs | Photodetectors |
| QD | Quantum Dots |
| GISAXS | Grazing Incidence Small Angle X-Ray Scattering |
| AFM | Atomic Force Microscopy |
| EQE | External Quantum Efficiency |
| WL | Wetting Layer |
| STM | Scanning Tunneling Microscopy |
| XAFS | X-Ray Absorption Fine Structure |
| FIB | Focused Ion Beam |
| WGPD | Waveguide Photodiode |
| OEIC | Optoelectronic Integrated Circuit |
| SCM | Sub-Carrier Multiplexed |
| LADAR | Laser Detection and Ranging |
| I-MSM | Inverted Metal–Semiconductor–Metal |
| RCE | Resonant Cavity Enhanced Photodetector |
| VM | Vollmer-Weber |
| ML | Monolayers |
| TEM | Transmission Electron Microscopy |

| | |
|---|---|
| STM | Scanning Tunneling Microscopy |
| APD | Avalanche Photodetector |
| PVD | Physical Vapour Deposition |
| CVD | Chemical Vapour Deposition |
| TE | Thermal Evaporation |
| SEs | Secondary Electrons |
| BSEs | Backscattered Electrons |
| RTA | Rapid Thermal Annealing |
| RTP | Rapid-Thermal Processors |
| RTO | Rapid-Thermal Oxidation |
| QE | Quantum Efficiency |
| FWHM | Full Width at Half Maximum |

## SIMULASI DAN FABRIKASI PENGESAN CAHAYA LOGAM-SEMIKONDUKTOR-LOGAM PULAU Ge DI ATAS Si

## ABSTRAK

Dalam kajian ini, eksperimen fabrikasi dan simulasi secara teori kepulauan Ge diatas Si berasaskan pengesan cahaya logam-semikonduktor-logam (MSM) telah dijalankan. Percikan frekuensi radio digunakan untuk mendeposit filem nipis Ge pada substrat silikon. Ini diikuti oleh pemanasan terma pantas untuk membentuk kepulauan Ge. Bukan hanya bahawa pemanasan menghasilkan pulau-pulau Ge tetapi juga lapisan nipis. Saiz dan ketumpatan pulau-pulau yang di hasilkan sangat dipengaruhi oleh masa pemanasan. Pengiraan kepadatan pulau menunjukkan bahawa peningkatan daripada sekitar $0.36\times10^{9}$ $cm^{-2}$ kepada $1.0\times10^{9}$ $cm^{-2}$ manakala ukuran saiz pulau-pulau tersebut menurun daripada 0.6 μm kepada 0.1 μm apabila waktu pemanasan meningkat dari 30s kepada 60s pada suhu 900˚ C. Pengesan cahaya MSM digunakan keatas sampel yang mempunyai pulau-pulau besar dan kecil dan pengukuran arus gelap, arus foto dan gandaan arus dilakukan pada suhu bilik untuk tujuan analisa. Kehadiran pulau-pulau Ge di atas lapisan nipis Ge telah terbukti memberikan kesan kepada pengesan cahaya MSM dimana ia mengurangkan arus gelap dan seterusnya meningkatkan gandaan arus. Dalam kajian ini, simulasi pengesan cahaya MSM keatas pulau-pulau Ge dan lapisannya telah dilakukan untuk mengesahkan keputusan eksperimen menggunakan simulator peranti Silvaco ATLAS. Keputusan simulasi telah mengesahkan keputusan eksperimen. Kajian simulasi secara mendalam telah dilaksanakan termasuk pasangan arus elektron-lohong, medan elektrik, aliran arus, transient dan sambutan spektra. Arus lohong telah mendominasi di dalam Ge dan kawasan tanpa lapisan Ge di antara celahan-celahan pengesan cahaya menunjukkan kesan sambutan spektra yang lebih baik. Sebagai tambahan, simulasi kuantum pengesan cahaya MSM untuk kepulauan Ge juga telah dijalankan, menunjukkan kepekatan elektron dan arus foto yang tinggi dan berbanding arus foto pada pengesan cahaya MSM silicon.

**SIMULATION AND FABRICATION OF Ge ISLANDS ON Si METAL-SEMICONDUCTOR-METAL PHOTODETECTORS**

**ABSTRACT**

In this thesis, experimental fabrication and theoretical simulation of Ge islands Si based metal-semiconductor-metal photodetectors have been reported. Radio frequency sputtering was used to deposit Ge thin films on silicon substrates. This is followed by rapid thermal annealing to form Ge islands. Not only that the annealing produces Ge islands but also wetting layer. The size and density of the islands are greatly influenced by the annealing time. An estimation of the island density shows that it increases from around $0.36\times10^9$ $cm^{-2}$ to $1.0\times10^9$ $cm^{-2}$ while the average size of the islands decreases from 0.6 μm to 0.1 μm when annealing time increases from 30 s to 60 s at 900 ˚C. Using these samples, metal–semiconductor–metal (MSM) photodiodes were fabricated for small and large islands. The performance of MSM devices were evaluated in terms of dark current, photocurrent and current gain measurements at room temperature. The presence of Ge islands and wetting layer structure has been shown to provide benefits for Si based MSM photodetectors; reducing the dark current and enhancement of current gain. Simulations of the Ge islands and wetting layer in MSM photodetectors have been performed to verify the experimental results using device simulator ATLAS in Silvaco in this thesis. Simulation results confirmed experimental results. A more detailed simulation studies has been conducted which show that hole current dominated in the Ge layers and device without wetting layer between the fingers which having the best transient response. In addition, the quantum simulation for Ge nanoislands MSM photodetector has been done, which shows high electron concentration and high photocurrent over typical Si MSM PD.

# CHAPTER 1

# INTRODUCTION

## 1.1 Overview

For more than 40 years, silicon (Si) has been the material of microelectronics. However, using of germanium (Ge) for microelectronics has gained more interest. The growth of Ge on Si is an appealing opportunity in order to combine proven semiconductor technology with a material exhibiting higher mobilities of charge carriers. It has been extensively studied from the viewpoint of fundamental physics and because of its technological importance. Ge on Si has been one of the most intensely investigated materials systems for the exploration of quantum dot self-assembly processes in misfit heteroepitaxial growth. In addition, this material system has attracted a wide interest since it can be exploited in the fabrication of new optoelectronic devices compatible with the well-developed Si technology [Stangl *et al.*, 2004]. It is well-known that Ge thin films grown on planar Si substrates follow a Stranski-Krastanov (S-K) mechanism due to the 4.17% lattice mismatch between Ge and Si and this led to form three-dimensional (3D) Ge islands on Si [Eaglesham *et al.* 1990, Mo *et al.* 1990, Jain *et al.* 2003]. There have been extensive studies on the size, morphology, structure, and chemistry of Ge islands grown on Si(100) and Si(001) substrates because of the great potential of Ge/Si self-assembled quantum dots for possible device applications [Kamins *et al.* 2007, Medeiros-Ribeiro *et al.* 1998, Chaparro *et al.* 2000]. Formation of these islands is characterized by their size, shape and density and these are necessary prerequisite for the use of self-assembled islands in future devices. To improve the performance of electronic devices, a considerable effort has to be devoted to control size uniformity, density and

positioning of the self-assembled nanostructures, as well as to shrink their dimensions [Goryll *et al*., 2003]. There have been several studies focused on the growth kinetics, electrical and optical characteristics of Ge islands on Si substrates under various growth conditions [Mota *et al*., 2002; Ratto *et al*., 2004; Chaparro *et al.,* 2000; Mo *et al.,* 1990].

Some studies have been done on the use of Ge nanoscaled lateral silicon/silicon–germanium layers, three-dimensional germanium quantum dots and Ge islands in semiconductor devices. Usually 3D islands are named quantum dots (QD) if their dimension is less than the exciton Bohr radius, (~ 24.3 nm in Ge). The heteroepitaxial self assembling of 3-D islands is one of the most promising paths towards the fabrication of QD devoted to nanoelectronics and nanophotonic applications. Ge quantum dots may find application in the field of quantum computation where they could be used to localize carriers forming quantum memory units (qbits) or perhaps used as single-photon emitters. Das *et al.* (2004) and Ray *et al.* (2005) reported a trilayer flash memory device structure using Ge nanocrystals embedded in a $SiO_2$ matrix deposited by radio frequency (RF) sputtering. In their studies, the appearance of strong and broad visible photoluminescence at room temperature is attributed to the quantum confinement of charge carriers in Ge nanocrystals having a wide distribution of crystallite sizes, making it attractive for future nanocrystals memory devices. Meanwhile, self-assembled Ge islands have been successfully incorporated into Si-based interband tunneling diodes and record peak-to-valley ratio Si-based tunnel diodes were achieved [Dashiell *et al.* 2002, Eberl *et al.,* 2000]. More recently, potential application is proposed, consisting in the incorporation of Ge islands into Si-based solar cells for more efficient light absorption [Alguno *et al.* 2003, Usami *et al.* 2004]. There is a limited literature on

using of Ge islands in metal-semiconductor-metal (MSM) photodetectors. A study has been done on MSM photodetector for Ge thin film showing that a $SiO_2$ passivation layer is required to reduce the high level of dark current [Buca *et al.* 2002]. In recent decades, MSM photodetectors have been studied due to their suitability for optical fiber communication application. The MSM structure plays an important role because of their high sensitivity-bandwidth product, fast response, simplicity, ease of fabrication, low dark currents, small capacitance, large active area for photodetection, low noise and the suitability for the monolithic integration of an optical receiver.

## 1.2 Literature Review

### 1.2.1 Ge islands

Formation of self-assembled Ge islands of various shapes like hut, pyramid and dome and their shape transitions have been fascinating [Mo *et al*. 1990, Medeiros-Ribeiro *et al.* 1998]. A technique to fabricate Ge islands is epitaxial growth, when lattice mismatch between Si and Ge (4.17%) and the overgrowth layer allows the formation of self-assembled quantum dots (QD) through the Stranski-Krastanov mechanism (SK). From the microscopic point of view, lattice mismatch is one of the most relevant factors which determines the growth mode. The growth of Ge/Si heterostructures has been intensely investigated due to the fact that Ge/Si lattice mismatch serves as a model system for the study of lattice-mismatched heteroepitaxy.

For better device performance, it is important to obtain islands of the same size, shape, and to find a mechanism for self-organized ordering. Despite the intensive research in the last few years, careful cataloging of the shape and size evolution of

the islands as a function of growth conditions has not yet been performed (Radić *et al.*, 2005). There are many growth parameters such as temperature, deposition rates, or growth interruptions, which affect the morphology and, hence, the electronic and optical properties of the islands.

Hartmann *et al.* (2005) has demonstrated the effects of the temperature and the amount of Ge on the morphology of Ge islands. In their work, the formation mechanisms and the structural features of Ge islands grown by Reduced Pressure–Chemical Vapor Deposition (CVD) onto Si(001) substrates have been studied. The size, the shape, and the density of Ge islands change drastically when altering parameters such as the growth temperature or the Ge coverage. For temperatures either equal to 600˚C or 650˚C, pyramids with {105} facets are nucleated first. They then gradually change into larger size domes as the amount of deposited Ge increases. Most probably because of longer Ge atoms diffusion lengths, the islands are less numerous (by a factor of 5) and larger (25% increase in diameter and height) at 650˚C than at 600˚C. At 550˚C, Ge hut clusters are nucleated first; then, small domes appear as the number of Ge monolayers increases. Those islands, although much denser, are rather smaller than the counterparts at higher temperatures. This study is the first time that such a systematic study of the structural and optical properties of Ge islands is carried out on an industrial Reduced Pressure CVD tool.

Stacked Ge islands which separated by Si spacers have been used in some structures. Stacking of Ge islands could increase the total volume of Ge in the structure without the introduction of misfit dislocations [Peng *et al.,* 1998]. Alguno *et al.* (2006) has investigated the influence of stacked Ge islands in the solar cell by the dark current–voltage (J–V) characteristics and the conversion efficiency of the solar cells with embedded stacked Ge islands in the intrinsic layer. These islands

were grown by molecular beam epitaxy on Si substrates. Results showed that the minority carrier diffusion and the recombination current components increase as a function of the stacked Ge island layers. This increase of the minority carrier diffusion current was due to an increase of the intrinsic carrier density as a function of the number of stacked layers. Similarly, the increase in the recombination current components was due to the enormous recombination of carriers in the intrinsic region as the number of stacked layer increases. This phenomenon could lead to a decrease of the open circuit voltage, $V_{oc}$. The decrease of $V_{oc}$ should be overcompensated by the increase of photocurrent, due to the presence of stacked Ge islands with higher absorption coefficient, in order to attain an optimum value of the conversion efficiency.

Alguno *et al.* (2003) reported the performance of solar cells with stacked self-assembled Ge dots in the intrinsic region of Si-based p-i-n diode. These dots were epitaxially grown on p-type Si(100) substrate via the Stranski-Krastanov growth mode by gas-source molecular beam epitaxy. Enhanced external quantum efficiency (EQE) in the infrared region up to 1.45 μm was observed for the solar cells with stacked self-assembled Ge dots compared with that without Ge dots. Furthermore, the EQE was found to increase with increasing number of stacking. These results show that electron-hole pairs generated in Ge dots can be efficiently separated by the internal electric field, and can contribute to the photocurrent without considerable recombination in Ge dots or at Ge/Si interfaces.

Usami *et al.* (2004) fabricated Si-based solar cell with stacked Ge islands grown via the Stranski–Krastanov growth mode in the intrinsic layer of p-i-n diodes. The onset of the external quantum efficiency in the near infrared regime was extended up to approximately 1.4 μm for the solar cells with stacked Ge islands. The

quantum efficiency was found to increase with increasing number of stacking, showing that a part of electron–hole pairs generated within Ge islands was separated by the internal electric field and contributed to the photocurrent. These results manifest that the Ge islands did play a role to increase the quantum efficiency.

Ge/Si heterojunction has been investigated and fabricated in some studies. Luana *et al.* (2001) demonstrated Ge/Si heterojunction photodetectors based on high quality epitaxial germanium grown on silicon. Germanium deposited by ultra-high-vacuum chemical vapor deposition (UHV-CVD) undergoes thermal annealing. It was demonstrated the effectiveness of post-growth thermal annealing and shown that the photodetectors exhibit record responsivity of 0.55 A/W and a sub-ns photoresponse at 1.3 μm in Ge/p-Si photodiode.

In other studies led by Ismail *et al.* (2006), the structural and photovoltaic (PV) characteristics of heteroepitaxial Ge film on monocrystalline Si (111) has been reported. The influence of Ge thickness and two types of annealing conditions on Ge/Si heterostructure and PV parameters have been investigated. The results of spectral responsivity at near IR region suggest that these heterojunctions are candidate to be used as detector for laser of $\lambda = 1.3$ μm.

Konle *et al.* (2003) fabricated silicon solar cells with embedded germanium layers to form three-dimensional islands in the Stranski–Krastanov growth mode. There are additional Ge-layers to increase the infrared absorption in the base of the cell to achieve higher overall photocurrent and overcome the loss in open circuit voltage of the heterostructure. Photocurrent measurements exhibit a higher response of the fabricated solar cells in the infrared regime compared to standard Si-cells.

In other study led by Konle *et al.* (2001) showed the influence of nanoscaled lateral silicon/silicon–germanium layers and three-dimensional germanium quantum

dots on the performance of silicon based infrared detectors in the wavelength range between 2 and 10 µm and solar cells for space applications. In addition, the growth of Ge islands on Si layers in the Stranski-Krastanov mode was performed to increase absorption and quantum efficiency in Si-solar cells.

There are few studies on the formation of Ge islands from Ge layer on Si substrate by post-growth annealing. Kovačević e*t al.* (2007) studied a thick Ge layer deposited on Si(100) held at 200˚C by thermal evaporation under high vacuum conditions. Upon subsequent thermal annealing in vacuum, self-assembled growth of nanostructural Ge islands on the Ge layer occurred by a Ge mass transport from the layer to the islands.

Pivac e*t al.,* (2006) studied a structural analysis of Ge islands on Si(100) substrates using grazing incidence small angle X-ray scattering (GISAXS). GISAXS is a nondestructive and powerful technique for structural characterization of islands fabricated on a substrate. In his work, the samples were prepared with high-vacuum evaporation of a 10 nm thick Ge layer on Si(100) substrate heated at 200˚C. The samples were annealed at 500–700˚C for 1 h in vacuum, yielding to island formation.

In similar study led by Pivac *et al.* (2006), a study of Ge islands formation on Si(100) substrates was presented using GISAXS and atomic force microscopy (AFM). Samples were prepared by magnetron sputtering of a 5 nm thick Ge layer in a very high vacuum on Si(100) substrate held at different temperatures. The optimum temperature for the islands formation was 650˚C. At this temperature, islands grow in conical shape with very similar dimensions; however, inter-island distances varied significantly.

Pervious discussions so far suggested one of the most important applications of Ge islands is in the incorporation of Ge islands into Si-based solar cells for more

efficient light absorption. The growth of Ge islands on Si in the Stranski-Krastanov mode was performed to increase absorption and quantum efficiency in Si-solar cells.

Ge islands have been grown by a number of methods such as molecular beam epitaxy (MBE) [Dvurechenskii *et al.,* 2005; Krasil *et al.,* 2002; Volodin *et al.,* 2004], ultra-high vacuum chemical vapor deposition (UHV-CVD) [Li *et al.,* 2004], low-pressure chemical vapor deposition (LPCVD) [Osipov *et al.,* 2005] and magnetron sputtering [Radic *et al.,* 2006]. The most common substrate to grow Ge nanostructures are Si(100) and Si(111).

Most of the reported quantum structures were prepared on Si(100) or Si(111) substrates using expensive tools such as molecular beam epitaxy (MBE) or high vacuum chemical vapor deposition (CVD) that are incompatible with high throughput solar cells fabrication. Some investigations reported the use of thermal evaporation [Das *et al.,* 2000].

A few studies use Ge islands in metal-semiconductor-metal (MSM) photodetector. In study led by Baharin [Baharin *et al.,* 2007], it has been shown that the presence of submicron and nano Ge islands grown using conventional method beneath the metal contact on Si substrate has double functions; suppressing the dark current and increasing the photocurrent. In many studies, one of the main reasons for using Ge is its high absorption. It was reported that layer of Ge have excellent potential for high-speed applications [Kawanaka *et al.,* 1996]. In another study, the hole transport across GaAs-Ge-GaAs heterovalent-interface via Ge islands was reported [Inada *et al.,* 1998]. Also in [Ahn *et al.,* 2007], it has been demonstrated high-speed and high efficiency Ge p-i-n photodetectors monolithically integrated with top coupled waveguides.

### 1.2.2 Ge wetting layer

A wetting layer is an initial layer of atoms that is epitaxially grown on a surface upon which self-assembled quantum dots or thin films are created. Although Ge/Si self-assembled islands are grown on top of the wetting layer (WL), some theoretical and experimental studies omit the WL from their simulations or investigations without much justification (Moutanabbir *et al.*, 2007). Others included the WL only briefly to discuss its influence on the properties of 3D islands. The wetting layer was taken into account in the earlier studies; however, the development of the wetting layer as well as the effects of the development on the island formation have been largely overlooked. The use of a wetting layer before dots formation has been demonstrated to be an important way of coherent growth of uniform and small dots (~10 nm) with a relatively high density (~$10^8$ to $10^{10}/cm^2$) [Miura *et al.,* 2000].

However, mass transport on the surface of WL underlies most of the other detailed mechanisms of islands nucleation and growth. Hence, a quantitative determination of WL–3D interdiffusion is of particular significance, both for improving our understanding of the microscopic mechanisms of self-organization, and also as a primary input for epitaxial growth models and calculations.

Rosei *et al.* (2000) studied formation of the wetting layer in Ge/Si(111) by scanning tunneling microscopy (STM) and X-ray absorption fine structure (XAFS). The evolution of the wetting layer has been followed up to its completion, both after and during deposition. The islands are flat and have a triangular shape with a lateral size which increases progressively with deposition. The growth law of the average dimensions of the islands and of the average number of islands per unit surface as a function of coverage has been studied.

Shi *et al.* (2005) reported the influence of boron on the formation of Ge quantum dots. The investigated structure consists of a Ge wetting layer, on which a sub-monolayer boron is deposited and subsequently a Ge top layer. For sufficiently thin Ge top layers, the strain field induced by boron on Ge wetting layer destabilizes the Ge top layer and causes the formation of small Ge quantum dots. In this study, the effect of boron on the Ge wetting layer was investigated.

Bernardi *et al.* (2006) studied the epitaxial growth of self-assembled Ge quantum dots when a sub-monolayer of carbon is deposited on a Ge wetting layer (WL) prior to the growth of the dots. Seta *et al.* (2009) investigated the island and wetting-layer intermixing in the Ge/Si(001) system upon capping. It was demonstrated that the island shape evolves at constant volume with silicon atom incorporation occurring in the absence of lateral diffusion of Ge and Si atoms from the wetting layer to the islands themselves. Portavoce *et al.* (2006), investigated the fundamental mechanism by which self-assembled Ge islands can be nucleated at specific sites on Si(001) using ultra-low-dose focused ion beam (FIB) pre-patterning. It was shown that the Ge wetting layer thickness depends on the density of template sites, and that it is lower than the value for an unmodified surface.

In some studies, particularly in the simulation, the wetting layer has been considered. Chiu *et al.* (2007) investigated the nanostructure formation of the Stranski-Krastanov (SK) systems by simulating the surface undulation of the systems driven by the surface diffusion mechanism. The particular interest is how the surface undulation leads to the development of faceted nanostructures and wetting layers. This study was carried out in three-dimensional simulation for the process. In this work, it has been presented a model for simulation of heteroepitaxial growth which is capable of reproducing various important phenomena observed in strained

heteroepitaxial growth. It was demonstrated that the appearance of a kinetic critical wetting-layer thickness can be explained on the basis of very few assumptions within the model. Liu *et al.* (2008) performed UHV-CVD experiments and theoretical calculations to investigate the mechanism of formation of the initial Ge wetting layer on Si(100)-2×1 reacted with the molecular hydride $GeH_4$. A precise Arrhenius temperature dependence was observed at the onset of growth of the Ge wetting layer and calculated the activation energy to be 30.7 kcal/mol for a 0.2-ML Ge coverage at temperatures ranging from 698 to 823 K.

### 1.2.3 Photodetectors

Photodetectors (PDs) are used in many applications of everyday life, from the bar code scanner at the grocery store to the receiver for a remote control, as well as the photoreceiver at the end of a fiber optic cable in an optical communication system. Photodetectors have been extensively studied both at the academia and industry levels. Most of the research has been focused and done on the optical to electrical conversion process. The photodetector is a key component in optical communication systems. Responsivity, quantum efficiency, rise time and bandwidth are the basic parameters which are used to characterize a photodetector and there is a need to improve these parameters.

The two major trends in PD development are aimed at developing a large bandwidth efficiency product and a high saturation current. Kato *et al.* (1999) first mentioned these trends and their limiting factors. Then several PD technologies based on the waveguide photodiode (WGPD) for these two trends were discussed.

Finally, they present a recently developed WGPD-based 50 Gb/s receiver optoelectronic integrated circuit (OEIC) technology.

DeCorby *et al.* (1999) discussed about the design of photodetectors with a balance of bandwidth, efficiency, and power handling capabilities which used in telecommunications and optoelectronics. Caria *et al.* (2004) has done responsivity measurements on commercial silicon photodetectors in the UV range, 200–400 *nm*. In his work, microstrip and pixel detectors have been used; also, they have performed measurements in back illumination geometry which is of particular interest in most industrial applications. Liu e*t al. (*1994) has proposed a metal-semiconductor-metal (MSM) photodetector with 100-nm finger spacing and width on a silicon-on-insulator substrate that has a scaled active layer, which were fabricated and characterized using electro-optic sampling. Buried oxide layer is important feature in speed enhancement of photodetectors which limits the active Si thickness. A bandwidth of 140 GHz at a wavelength of 780nm was achieved by using this model. Good metal-semiconductor Schottky contact and low detector dark current are the results for this condition.

One of the most important factors in photodetectors is quantum efficiency which related to light absorption in photodetectors. Collin *et al.* (2004) proposed a new technique for efficient light absorption in MSM photodetectors. In his work, it is shown that the strong confinement of light in sub-wavelength metal-semiconductor gratings can be achieved by Fabry-Perot resonances involving vertical transverse magnetic and transverse electric guided waves, thereby increasing the quantum efficiency in device.

In the past few years, there has been a growing interest increased interest in MSM photodetectors has developed due to its low capacitance and high speed. Using

these detectors for optical communication receiver has been fabricated with integrated circuits. Liu *et al.* (1993) demonstrated a novel monolithic integrated optoelectronic mixing receiver with low conversion loss. This configuration of optoelectronic mixer can be applied for a wideband sub-carrier multiplexed (SCM) distribution system in GHz range with a suitable laser diode and photodetector. Recently, an MSM detector has been utilized as an optoelectronics mixer in a frequency modulated continuous-wave laser detection and ranging (LADAR) system [Shen *et al.,* 2000].

The response speed of an MSM photodetector is largely limited by the transit time of the photogenerated carriers, and thus, the inter-electrode spacing should be small. Reducing the finger spacing and finger width of an MSM PD can greatly increase its speed and sensitivity. Liu *et al.* (1992) fabricated MSM PD's with finger spacing and width as small as 25 nm on bulk GaAs, low-temperature-grown-GaAs, and bulk Si, using a custom-built electron-beam lithography. In his work, it has been demonstrated an MSM photodetector with finger spacing smaller than the wavelength of the light. Seo *et al.* (2004) demonstrated an Inverted metal–semiconductor–metal (I-MSM) photodetectors, which are thin-film MSMs with the growth substrate removed and fingers on the bottom of the device (to eliminate finger shadowing to enhance responsivity) for high-speed high-efficiency large-area photodetectors. Lee *et al.* (1995) have proposed a novel high-speed silicon photodetector that operates at a wavelength of 830 nm which consists of a Metal-Semiconductor-Metal (MSM) detector that is fabricated on a 5-μm thick silicon membrane.

A resonant cavity enhanced photodetector (RCE) provides wavelength selectivity in detection. The principle of resonant-cavity enhanced photodetectors is

that a fast photodetector was put into a Fabry-Perot (FP) cavity to enhance the signal magnitude. These detectors can function as channel discriminators in wavelength division multiplexing systems [Kishino *et al.,* 1996]. This is achieved by utilizing reflectors around the active region. The photons make multiple passes across the active region, improving the probability of absorption, thereby increasing the quantum efficiency. A general expression for efficiency of RCE photodetectors was derived while taking the external layer losses into account for the first time.

Some attempts have been aimed at improving the Si MSM detector quantum efficiency at visible and near IR wavelengths by fabricating vertical and U-shaped trench electrodes using reactive ion etching and wet chemical etching methods [Ho *et al.,* 1996; Liah *et al.,* 1998]. For an MSM photodetector, the amount of energy reaching the interface of the detector should be a maximum and this depends on the geometric and optical parameters of the structures as well as on the properties of the incident radiation (wavelength, polarization, angle of incidence, and the like). In the work by Kuta *et al.* (1994) photocurrent and transmission studies of metal-semiconductor-metal (MSM) photodetectors on semi-insulating GaAs substrates demonstrate a polarization and wavelength dependence of the coupling of light into the metal electrodes.

Optoelectronic integrated circuits are very promising for use in optical communication systems because of their high performance characteristics and small size. Circuit simulations of electronic circuits and photodetectors must be conducted for enhancing their performance. Sano (1990) proposed an analytical model based on the behavior of photo-generated carriers and electric fields. This model was implemented on a SPICE (Simulation Program with Integrated Circuit Emphasis) like circuit simulator and was found to be useful for designing high performance

optoelectronic receivers. More simulation models have to be developed in order to improve the optical transmission characteristics.

Poisson's equation, current-continuity equations, and a rate equation for charged traps are numerically solved in two dimensions, to explain the behavior of photo-generated carriers and electric fields in metal-semiconductor-metal photodetectors (MSM PDs). Sano (1990) proposed an analytical model on the basis of these solutions and implemented in a SPICE-like circuit simulator.

Finally, there is a need to study Ge on Si photodetectors due to the excellent optoelectronic properties.

## 1.3 Research Objectives

The main objectives of this thesis are the following:

1) To grow Ge islands with different sizes using sputtering techniques,

2) To fabricate MSM photodetector based on Ge islands,

3) To investigate the effects of Ge islands in MSM PD using both experimental and simulation procedure,

4) To investigate the effect of Ge wetting layer in Si MSM PD using device simulator.

5) To simulate the Ge Nanoislands MSM Photodetector with quantum model.

## 1.4 Organization of Thesis

The reminder of this thesis is organized in the following manner which are shortly described below.

The next chapter serves as some theories about the work. Ge optical and electrical properties and Ge islands were explained. The end of the chapter some theoretical description of MSM photodetectors were given.

The third chapter focuses on experimental procedure of the related work. Here the film deposition methods are described. This included the physical deposition methods; thermal evaporation and radio frequency (RF) sputtering. The next part of this chapter explains used instruments through the work. In addition, the end of the chapter, the simulator software (Silvaco) and simulation procedure were described, which have used in this work.

The fourth chapter of this thesis is the results and discussion of the study of Ge islands on Si MSM PDs performance.

The fifth chapter of this thesis is the results and discussion of the simulation of the role of Ge wetting layer in Si MSM photodetector.

The sixth chapter of this thesis is the results and discussion of the simulation of Ge islands MSM PD without Ge wetting layer by quantum model.

We will conclude this thesis and discuss future work in chapter 7. Conclusion presented in this chapter, gives a brief overview of the research and the achieved results also the future works suggests a perspective of the future researches that can be implemented based on the outcomes of this thesis.

# CHAPTER 2

# THEORY

## 2.1 Introduction

The solids known as semiconductors have been the subject of very extensive research over recent decades. Semiconductors are a group of materials having electrical conductivities (in the range of $10^4$ to $10^{-10}$ $(\Omega\ cm)^{-1}$) between metals and insulators ($s=10^{-10}$ to $10^3$ $(\Omega\ cm)^{-1}$). The conductivity of these materials can be varied over orders of magnitude by changes in temperature, optical excitation, and impurity content. This variability of electrical properties makes the semiconductors as a natural choice for electronic device. The column IV semiconductors, silicon and germanium are called elemental semiconductors because they are composed of single species of atoms. Every solid has its own characteristic energy band structure. This variation in band structure is responsible for the wide range of electrical characteristics observed in various materials. Semiconductor materials at 0 K have basically the same structure as insulators. In metals, the bands either overlap or are only partially filled. Thus in metals, high electrical conductivity is due to the fact that electrons and empty energy states are intermixed within bands so that electrons can move freely under the influence of an electric field [Streetman *et al.,* 2006].

## 2.2 Electrical and Optical Properties of Ge

Germanium is an elemental semiconductor that was used to fabricate the first transistors and solid state devices. The common solid phase of Ge is crystalline with

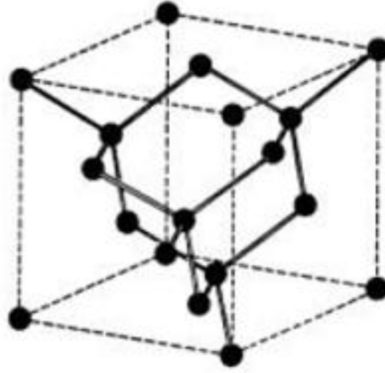

Figure 2.1: Crystalline structure of Ge showing the tetrahedral arrangement of the bonds.

a covalently bonded diamond structure, i.e. each atom has a coordination number of four (nearest neighbors) and a tetrahedral binding angle of 109.28º as schematically drawn in fig. 2.1. Energetically, this structure has the lowest free energy and is therefore the most stable one since the perfect lattice does not give rise to strain energy. The extension of the symmetry of this structure defines the quality of the crystal which is called polycrystalline when composed of different crystalline regions (grains).

Table 2.1 lists the most important electrical properties of bulk crystalline Ge. Notice that some properties are very different when film form. The properties of the liquid or the amorphous phase are also different. Ge is an excellent candidate to replace Si photodetectors [higher mobility and high absorption]. The band gap of Ge, like that of Si is also indirect. Alloys of Si and Ge are thus also indirect band gap materials. Ge has the direct transition at 0.805 eV, corresponding to 1550 nm and indirect transition at 0.66 eV. At 850 nm the absorption coefficient of Ge is mid-tens of thousands/cm as in fig. 2.2. Thus, Ge has the absorption coefficient more than two orders of magnitude larger than Si. Furthermore, table 2.1 shows comparison of electronics properties of Ge and Si [Sze, 2002]. Mobility of Ge is much higher than that of Si, especially hole mobility.

Table 2.1: Band structure parameters for the indirect gap element Germanium. $\boldsymbol{E_g^{ind}}$ is indirect band gap; $\boldsymbol{E_g^{dir}}$ direct band gap at the Γ point. [Streetman *et al.,* 2006, Pavesi *et al.,* 2006].

| **Property** | **Germanium** | **Silicon** |
|---|---|---|
| $E_g^{ind}$ (ev) (300 k) | 0.66 | 1.1 |
| $E_g^{dir}$ (ev) (300 k) | 0.805 | 3.4 |
| Electron mobility ($cm^2V^{-1}s^{-1}$) | 3900 | 1500 |
| Hole mobility ($cm^2V^{-1}s^{-1}$) | 1900 | 600 |

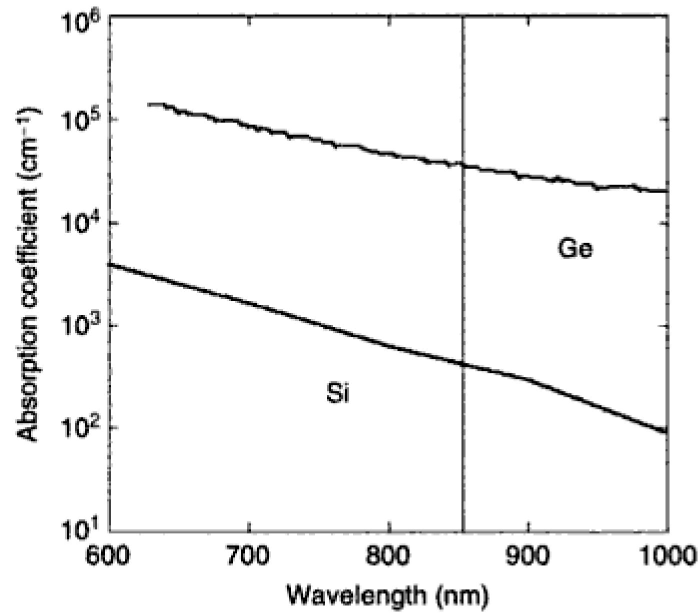


Figure 2.2: Absorption coefficients of Si and Ge [Pavesi *et al.,* 2006].

The band gap represents the minimum energy difference between the top of the valence band and the bottom of the conduction band, however, the top of the valence band and the bottom of the conduction band are not generally at the same value of the electron momentum. In a direct band gap semiconductor, the top of the valence band and the bottom of the conduction band occur at the same value of

momentum, as shown in fig 2.3(a). In an indirect band gap semiconductor, the maximum energy of the valence band occurs at a different value of momentum to the minimum in the conduction band energy, as shown schematically in fig. 2.3 (b). Transitions at the band edge must therefore involve a large change in the electron wave vector. Optical frequency photons only have a very small k vector, and it is not possible to make this transition by absorption of a photon alone: the transition must involve a phonon to conserve momentum.

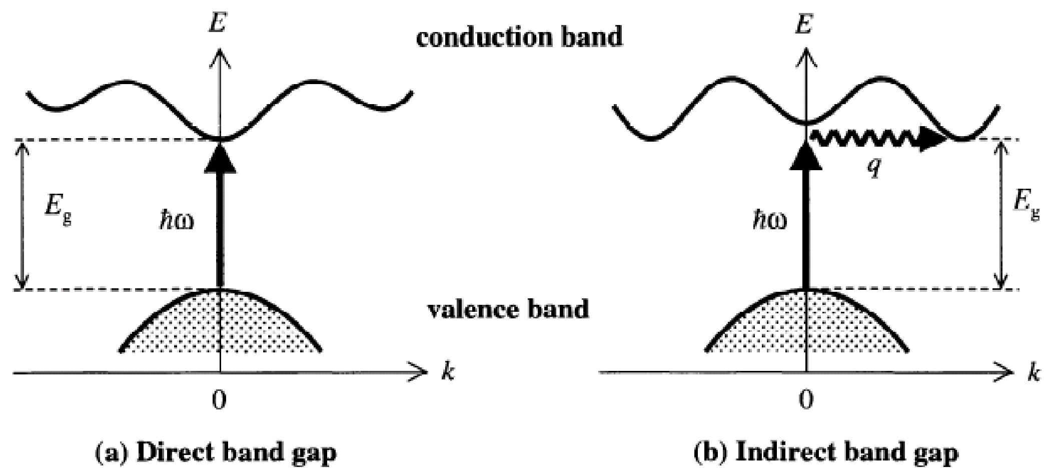


Figure 2.3: Inter-band transitions in solids: (a) direct band gap, (b) indirect band gap. The vertical arrow represents the photon absorption process, while the wiggly arrow in part (b) represents the absorption or emission of a phonon [Fox, 2001].

Indirect absorption has been thoroughly studied in materials like germanium. The band structure of germanium is shown in fig. 2.4. The lowest conduction band minimum of germanium occurs at the L point, where k = $\frac{\pi}{a}$ (1, 1, 1), and not at k = 0. This makes germanium an indirect gap semiconductor. The value of the indirect gap is 0.66 eV, which corresponds to the band gap determined by electrical measurements. This is 0.14 eV smaller than the direct gap at k = 0.

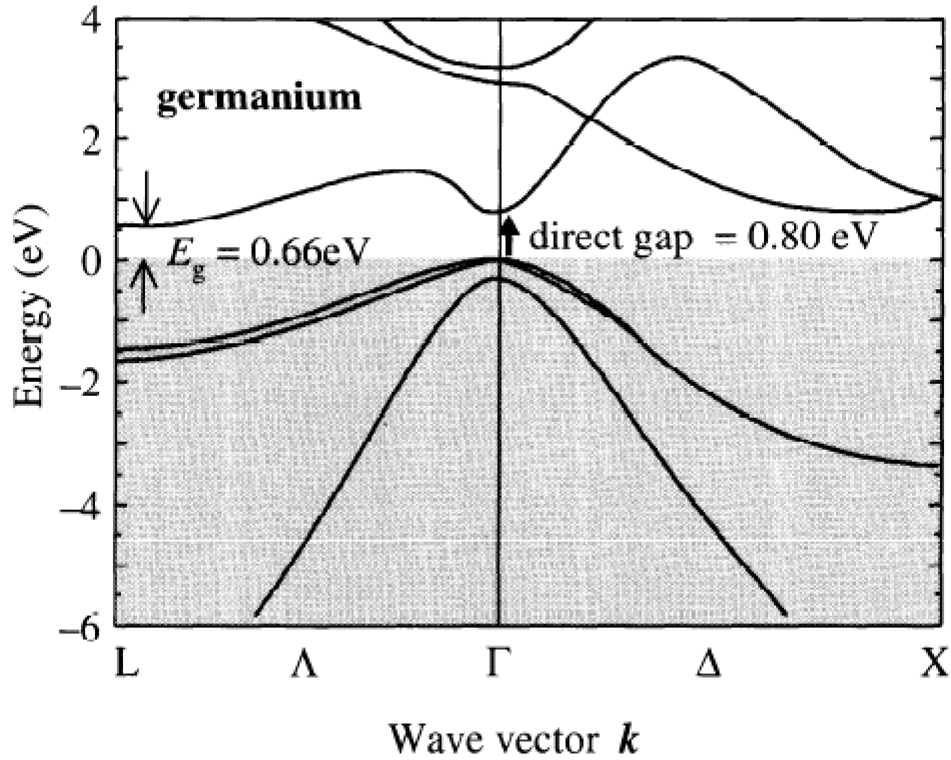


Figure 2.4: Band structure of Germanium (Energy vs. wave vector) [Fox, 2001].

Figure 2.5 shows the results of absorption measurements on germanium at room temperature. $\sqrt{\alpha}$ is plotted against ħω in the spectral region close to the band gap at 0.66 eV. The data fits well to a straight line, which confirms the prediction in the following equation:

$$\alpha^{\text{indirect}}(\hbar\omega) \propto (\hbar\omega - E_g \mp \hbar\Omega)^2 \quad (2.1)$$

This shows that we expect the absorption to have a threshold close to $E_g$, but not exactly at $E_g$. The difference is $\mp\hbar\Omega$, depending on whether the phonon is absorbed or emitted. The data extrapolates back to 0.65 eV, which indicates from eq. (2.1) that a phonon of energy ~ 0.01 eV has been absorbed. The wave vector q of the phonon must be equal to that of an electron at the L-point of the Brillouin zone.

The energies of the four different phonon modes with the required wave vector are listed in table 2.3, from where we see that it must be TA phonons that are involved. The experimental data also shows a tail extending down to about 0.60 eV. This is caused by absorption of the higher frequency phonons and also multiphonon absorption [Fox, 2001].

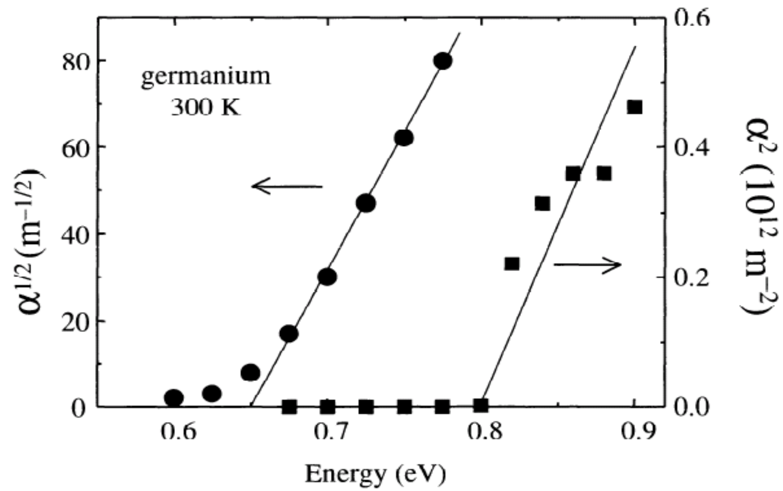


Figure 2.5: Experimental data for the absorption coefficient of germanium at room temperature [Fox, 2001].

Table 2.2: Phonon energies for germanium at the L point where q = $\frac{\pi}{a}$ (1,1,1), a being the unit cell size.

| **Mode** | **ħΩ** |
|---|---|
| Longitudinal acoustic (LA) | 0.027 |
| Transverse acoustic (TA) | 0.008 |
| Longitudinal optic (LO) | 0.030 |
| Transverse optic (TO) | 0.035 |

## 2.3 Growth Modes

### 2.3.1 Film growth mode

A technology closely related to crystal growth involves the growth of single-crystal semiconductor layers on a single-crystal semiconductor substrate. This is called epitaxy, from the Greek words epi (meaning "on") and taxis (meaning "arrangement"). The epitaxial layer and the substrate materials may be the same, giving rise to homoepitaxial. Epitaxy or epitaxial growth is the process of depositing a thin layer (0.5 to 20 microns) of single crystal material over a single crystal substrate. In semiconductors, the deposited film is often the same material as the substrate, and the process is known as homoepitaxy, or simply, epi [Sze, 2002].

The details of the growth modes for the simplest case of homoepitaxy, the growth of a film on a single-crystalline surface of the same material, is indicated in fig. 2.6.

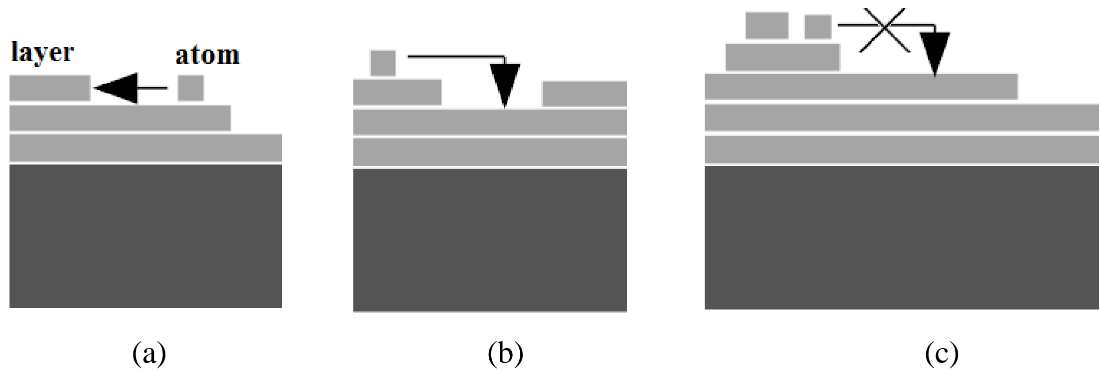


(a) (b) (c)

Figure 2.6: Growth modes of homo-epitaxy: (a) step-propagation, (b) 2d-islands growth, and (c) multi layer growth [Waster, 2005].

Step-propagation dominates at high temperatures (fig. 2.6(a)) and two-dimensional islands growth will predominate if immobile clusters are formed by the encounters of mobile adatoms (fig 2.6(b)). Also, if the jump across the step is kinetically hindered multilayer growth will be observed (fig. 2.6(c)).

If we want to grow an epitaxial film on a different substrate (so-called heteroepitaxy), two material parameters have to be considered in addition: the surface energy, $\gamma$, and the lattice parameter or lattice match of the two materials. For the case of good lattice match the difference in surface energy leads to two different growth modes as indicated in fig. 2.7. It is well known that there are three types of growth modes for heterogeneous epitaxial growth (which including the Ge/Si system): the Frank-Van der Merwe [Frank *et al.,* 1949], Stranski-Krastanov [Stranski, 1939], and Volmer-Weber [Volmer, 1926] modes, which are named after the original researchers.

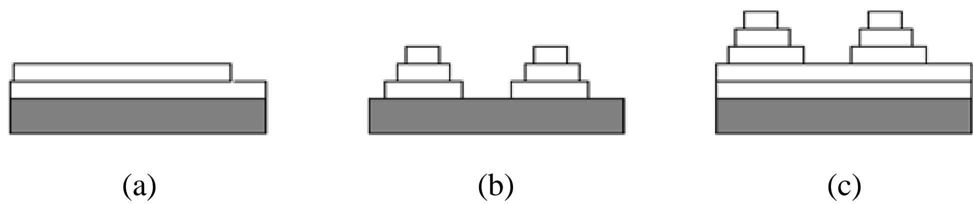

(a) (b) (c)

Figure 2.7: Growth modes of hetero-epitaxy: (a) Frank-van der Merwe (FM) (b) Vollmer-Weber (VM) (c) Stranski-Krastanov (SK) [Waster, 2005].

The typical layer-by-layer growth is referred to as Frank-Van der Merwe (FM) growth, which is required to fabricate high-quality large films for practical applications. In this mode a low surface energy adsorbate wets the substrate with a continuous film and higher layers do not start growing until the topmost one is nearly complete.

$$\gamma_{substrate} \geq \gamma_{layer} + \gamma_{substrate/layer} \tag{2.2}$$

Eq (2.2) shows the perfect wetting and pure layer by layer or frank-van-Merve growth.

For some heterogeneous epitaxial growth conditions, where there is, for example, a substantial lattice mismatch, layer-by-layer growth is impossible and only 3D islands are formed. This growth is referred to as Volmer-Weber (VW) growth.

$$\gamma_{\text{substrate}} \leq \gamma_{\text{layer}} + \gamma_{\text{substrate/layer}} \tag{2.3}$$

For this consideration the surface energies of the crystallographic orientations of actual interest must be applied, which are often not available in data reference tables.

If there is a lattice mismatch between substrate and film, an additional growth mode may be observed as indicated in fig. 2.7(c) Stranski-Krastanov growth which is an intermediate mode where growth starts in a layer-to-layer mode during the first few atomic layers, and then form 3D islands beyond a certain thickness, which is usually referred to as critical thickness. A first layer may grow matched to the substrate, which yields additional strain energy. With growing thickness this strain energy increases in proportion to the strained volume and an island formation may become more favorable in spite of the larger surface area. In Stranski-Krastanov (SK) mode, the first adsorbate layer reduces the substrate surface energy enough to stop the wetting behavior, and the growth continues as 3D islands. Based on thermodynamic analysis, the growth mode in a given system is determined from the surface/interface energy and the lattice mismatch which mentioned above.

Two of these three equilibrium growth modes (SK and VW) can produce self-assembled nanodots, Ge pyramids on Si surfaces being, perhaps, the most famous example. Self-organization in such systems is typically limited to nearest-neighbor interactions, but can become significant in multilayer systems.